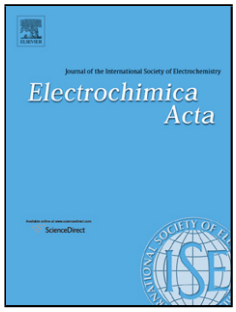

Title: The effect of pH on the electrocatalytic oxidation of formic acid/formate on platinum: A mechanistic study by surface-enhanced infrared spectroscopy coupled with cyclic voltammetry

Author: Jiyong Joo Taro Uchida Angel Cuesta Marc T.M. Koper Masatoshi Osawa

PII: S0013-4686(14)00342-9
DOI: http://dx.doi.org/doi:10.1016/j.electacta.2014.02.040
Reference: EA 22201

To appear in: *Electrochimica Acta*

Received date: 11-11-2013
Revised date: 10-1-2014
Accepted date: 8-2-2014

Please cite this article as: J. Joo, T. Uchida, A. Cuesta, M.T.M. Koper, M. Osawa, The effect of pH on the electrocatalytic oxidation of formic acid/formate on platinum: A mechanistic study by surface-enhanced infrared spectroscopy coupled with cyclic voltammetry, *Electrochimica Acta* (2014), http://dx.doi.org/10.1016/j.electacta.2014.02.040

The effect of pH on the electrocatalytic oxidation of formic acid/formate on platinum: A mechanistic study by surface-enhanced infrared spectroscopy coupled with cyclic voltammetry

Jiyong Joo,[1,2] Taro Uchida,[2] Angel Cuesta,[3,§] Marc T.M. Koper,[2,4] Masatoshi Osawa*[,2]

[1] Graduate School of Chemical Sciences and Engineering, Hokkaido University, Sapporo 060-8682, Japan

[2] Catalysis Research Center, Hokkaido University, Sapporo 001-0021, Japan

[3] Instituto de Química Física "Rocasolano", CSIC, C. Serrano 119, E-28006 Madrid, Spain

[4] Leiden Institute of Chemistry, Leiden University, 2300 RA Leiden, The Netherlands

* Corresponding author. E-mail address: osawam@cat.hokudai.ac.jp (M. Osawa)

[§] Present Address. Department of Chemistry, School of Natural and Computing Sciences, University of Aberdeen, Aberdeen AB24 3UE, UK.

Abstract

The electrocatalytic oxidation of formic acid (HCOOH) and formate ($HCOO^-$) to CO_2 on platinum has been studied over a wide range of pH (0–12) by surface-enhanced infrared absorption spectroscopy (SEIRAS) coupled with cyclic voltammetry. The peak current of HCOOH/$HCOO^-$ oxidation exhibits a volcano-shaped pH dependence peaked at a pH close to the pK_a of HCOOH (3.75). The experimental result is reasonably explained by a simple kinetic model that $HCOO^-$ oxidation is the dominant reaction route over the whole pH range. HCOOH is oxidized after being converted to $HCOO^-$ via the acid-base equilibrium. The ascending part of the volcano plot at pH < 4 is ascribed mostly to the increase of the molar ratio of $HCOO^-$, while the descending part at pH > 4 is ascribed to the suppression of $HCOO^-$ oxidation by adsorbed OH or oxidation of the electrode surface. In acidic media, HCOOH is

adsorbed on the electrode as formate with a bridge-bonded configuration. The bridge-bonded adsorbed formate is stable and suppresses $HCOO^-$ oxidation by blocking active site. However, the suppression is not fatal because bridge-bonded adsorbed formate enhances the oxidation of $HCOO^-$ at high potential by suppressing the adsorption of OH or surface oxidation. The complex cyclic voltammograms for HCOOH/$HCOO^-$ oxidation also can be well interpreted in terms of the simple kinetic model. The experimental results presented here serve as a generic example illustrating the importance of pH variations in catalytic proton-coupled electron transfer reactions.

1. Introduction

The direct formic acid fuel cell (DFAFC) is a promising power source [1-4]. Owing to this technological importance, electrooxidation of formic acid (HCOOH) taking place at the anode catalyst in DFAFC has been studied intensively, especially in acidic media. This reaction has also attracted much interest in fundamental research as a simple model electrocatalytic system. Nevertheless, the mechanism of HCOOH oxidation is still matter of discussion.

It is generally accepted that HCOOH is oxidized to CO_2 via a dual pathway mechanism composed of a main reaction pathway via an adsorbed active intermediate and a pathway involving an adsorbed poisoning species that is oxidized to CO_2 at high overpotentials [5-7]. The poisoning species was identified to adsorbed CO in the 1980s by using infrared reflection absorption spectroscopy (IRAS) [8], while no other adsorbed species had been detected until Miki et al. [9] observed the adsorption of a formate species that is bonded to the surface via two oxygen atoms (bridge-bonded adsorbed formate) by employing surface-enhanced infrared absorption spectroscopy in the attenuated total reflection mode (ATR-SEIRAS) [10, 11]. Through systematic ATR-SEIRAS studies combined with electrochemical measurements, Samjeské et al. [12-15] and Cuesta et al. [16, 17] proposed

bridge-bonded adsorbed formate as the intermediate in the main non-CO pathway (termed hereafter as *bridge-bonded adsorbed formate pathway*). Further, Cuesta et al. [16, 18] suggested that the bridge-bonded adsorbed formate is the intermediate common to the CO and non-CO pathways. On the other hand, Chen et al. [19-21] claimed that bridge-bonded formate is a site-blocking spectator and HCOOH is directly oxidized to CO_2 via a weakly adsorbed molecular HCOOH precursor (termed as *direct HCOOH pathway*), which led them to propose a triple pathway mechanism by adding direct HCOOH pathway to the dual pathway mechanism. All these studies employed the same experimental techniques (ATR-SEIRAS combined with cyclic voltammetry) and obtained essentially identical results. The two different reaction mechanisms proposed by Samjeské et al. [12-15] and Cuesta et al. [16, 17], on the one side, and by Chen et al. [19-21], on the other side, stem from the different interpretations of the nonlinear relationship between the oxidation current and the band intensity of bridge-bonded adsorbed formate (approximately proportional to coverage). Recently, Grozovski et al. [22] reported that the oxidation current is proportional to the coverage of adsorbed formate determined by fast cyclic voltammetry and concluded that adsorbed formate is the intermediate in HCOOH oxidation.

A similar disagreement exists also in theoretical studies of the mechanism of this reaction. Neurock et al. [23] and Wang and Liu [24] concluded that the bridge-bonded adsorbed formate pathway is energetically much less favorable than direct HCOOH pathway, while Gao et al. [25] concluded that bridge-bonded adsorbed formate pathway is slightly more favorable than direct HCOOH pathway.

In recent years, the electrocatalytic oxidation of small organic molecules in alkaline media has received renewed interest due to the recent advent of alkaline anion exchange membranes for alkaline fuel cells. HCOOH is a weak acid with a pK_a of 3.75 [26] and exists mostly as formate ($HCOO^-$) in alkaline media. John et al. [27] and Jiang et al. [28]

investigated the oxidation of $HCOO^-$ on Pt in strong alkaline media and proposed a dual and triple pathway mechanisms, respectively, analogous to those of HCOOH oxidation. $HCOO^-$ oxidation in alkaline media is well known to be very slow compared to HCOOH oxidation in acidic media. Interestingly, however, Buck and Griffith [29], Bagotsky and Vassiliyev [30], Beden et al. [31], Adzic et al. [32], Kita et al. [33], and Haan and Masel [34] have shown that the oxidation current on Pt or Pd increases with increasing pH in the pH range between 1 and 5, i.e., with increasing the molar ratio of $HCOO^-$. Considering that solving this puzzle could lead to full understanding of reaction mechanisms involved, we systematically investigated the pH dependence of HCOOH/$HCOO^-$ oxidation in a wide pH range from 0 to 12 by cyclic voltammetry and found that the oxidation current is maximal at a pH close to the pK_a of HCOOH, as shown in Fig. 1 [35]. We additionally found that the experimental result can be reasonably explained by assuming that $HCOO^-$ is more reactive than HCOOH and that HCOOH is oxidized after being converted to $HCOO^-$ via the acid-base equilibrium. To understand the reaction comprehensively, however, detailed study on the CO pathway is also indispensable. Since adsorbed CO gives very strong infrared absorption bands, ATR-SEIRAS that enables time-resolved monitoring of the electrode surface during the reaction is very suited for this purpose. In the present study, the pH dependence of HCOOH/$HCOO^-$ oxidation is examined by ATR-SEIRAS coupled with cyclic voltammetry and the reaction is discussed in more detail by integrating the present SEIRAS study and the kinetic study reported in our previous publication [35].

The significance of the present study goes beyond this relatively simple electrocatalytic system because many electrocatalytic reactions are strongly pH dependent and the pH dependence must be related to the decoupling of proton and electron transfer at some stage in the reaction mechanism [36-38]. Recently, such an effect was shown to be important for predicting the optimal pH for electrooxidation of alcohols on gold electrodes [39]. We will

show that the experimental results presented here serve as a generic example highlighting the importance of pH variation in catalytic proton-coupled electron transfer reactions.

2. Experimental

Protons produced by the oxidation of HCOOH/$HCOO^-$ can change the pH at the interface and can provoke a considerable change in the molar ratio of HCOOH and $HCOO^-$, especially in the pH range around the pK_a. To avoid such an effect, 0.2 M phosphate buffer solutions (pH 1.5-12), prepared from H_3PO_4, NaH_2PO_4, Na_2HPO_4, and/or Na_3PO_4, were used as the electrolyte solution. All solutions were made using 18 MΩ cm Milli-Q water. As the HCOOH/$HCOO^-$ source, HCOONa was added to the electrolyte solutions to 20 mM. The solutions were deaerated with Ar before each experiment. All chemicals were analytical grade ones purchased from Wako Pure Chemicals (Tokyo) and used as received.

Experimental details of ATR-SEIRAS were described elsewhere [11, 40]. A glass cell, equipped with a Pt gauze counter electrode and an Ag/AgCl (sat'd KCl) reference electrode separated from the working electrode via a Luggin capillary, was used for the spectroelectrochemical measurements. The working electrode was a Pt thin film formed on the totally reflecting plane of a Si triangle prism (Pier Optics, Tatebayashi, Japan) by a chemical deposition technique [9, 41]. Prior to the measurements, the electrode surface was cleaned in the supporting electrolyte solution without HCOOH/$HCOO^-$ by repetitive potential scans between the surface oxidation and the hydrogen adsorption regions until a stable cyclic voltammograms (CV) was obtained. A potentiostat (EG&G PAR, model 263A) was used in controlling the electrode potential and recording CVs. Although the electrode potential was measured against the Ag/AgCl reference electrode, all potentials in this paper are referred to the standard hydrogen electrode (SHE), unless otherwise noted.

A Fourier transform infrared spectrometer (Bio-Rad, FTS-60A/896) equipped with a MCT detector and a homemade single reflection accessory (angle of incidence of 60°) was used in recording the ATR-SEIRA spectra of the electrode surface. The spectral resolution used was 4 cm^{-1}. Spectra were sequentially acquired at every 2 s interval (time required for co-adding 10 interferograms) during a potential scan at 20 mV s^{-1}, while a CV was recorded simultaneously. Therefore, a spectrum is an average over a 40 mV interval. A single beam spectrum collected in advance in the pure supporting electrolyte at a potential in the hydrogen adsorption region was used as reference for calculating the spectra. All spectra are shown in absorbance units. All experiments were carried out at room temperature.

3. Results and discussion

3.1 SEIRA spectra and cyclic voltammograms

Figure 2a shows a series of SEIRA spectra of the surface of a Pt thin-film electrode in 0.2 M H_3PO4 (pH 1.5) containing 20 mM HCOONa collected during a potential scan from 0 to 1.2 and back to 0 V at 20 mV s^{-1}. A single beam spectrum collected at 0 V in the HCOONa-free solution in advance was used as the reference. At the beginning of the potential scan (i.e., at 0 V), the spectrum is dominated by a very strong band at 2050~2070 and a medium strong band at ~1850 cm^{-1} assigned to linear CO (CO_L) and bridge-bonded CO (CO_B), respectively. The dip at 1610 cm^{-1} is the bending mode of water that was removed from the interface upon adsorption of CO [42]. The CO bands disappear at around 0.8 V due to the oxidative removal of CO_{ads} and a new band emerges at 1325 cm^{-1} at around 0.5 V. This band has been assigned to the symmetric O–C–O stretching mode of bridge-bonded adsorbed formate [9], while the asymmetric O–C–O stretching mode of the bridge-bonded adsorbed formate, expected around 1590 cm^{-1}, is not observed in the spectra due to the surface selection rule in SEIRAS [43]. The broad band at ~ 1050 cm^{-1} that emerges after CO_{ads} being oxidized

completely are a P-O stretching vibration of phosphate adsorbed on the electrode surface ($H_2PO_4^-$ and/or HPO_4^- [44]). The spectral changes are reversed during the subsequent negative-going scan. Since the IR absorption enhancement is limited mostly to adsorbed species [10, 11], the absorption bands of HCOOH, the dominant species in the bulk solution, are absent in the spectra (for example, ν(C=O) expected around 1700 cm^{-1}). The spectral range below 950 cm^{-1} was not accessible due to the strong absorption of the Si prism.

The CV collected simultaneously with the SEIRA spectra is shown in Fig. 2b (top panel). The dotted trace is the CV of the electrode recorded in the same electrolyte solution without HCOONa. In the positive-going scan from 0.0 V, two oxidation peaks (p1 and p2) appear, while a peak and two shoulders (p3, p4, and p5) appear in the negative-going scan after the reduction of the oxide on the electrode. The labels of the peaks or shoulders follow their order of appearance.

For a comparison of the CV and the SEIRA spectra, the integrated band intensities of the CO_L, CO_B, and bridge-bonded adsorbed formate are plotted as a function of the applied potential in the same figure (bottom panel). The results are essentially identical to those obtained in H_2SO_4 [13, 14], but it is worthwhile to review them for the sake of a comparison with $HCOO^-$ oxidation in neutral and alkaline media described later. The electrode surface is almost fully covered by CO_{ads} at the beginning of the potential scan as evidenced by the complete absence of the hydrogen desorption peaks in the CV. In the potential range where peak p1 appears, the band intensities of CO_L and CO_B are almost constant. However, a previous SEIRAS study of CO_{ads} stripping has revealed that 10–20% of CO_L is oxidized in this potential range (the so-called pre-oxidation) [45]. The disagreement between spectroscopy and electrochemistry is due to the saturation of the IR band intensity at high CO_{ads} coverage. The partial CO_{ads} oxidation uncovers some amount of active sites, and enables HCOOH oxidation and also the adsorption of bridge-bonded formate. At higher

potentials around 0.7 V, both CO_L and CO_B are oxidized and completely removed at 0.8 V, which sharply increases bridge-bonded adsorbed formate to reach a maximum at ~0.8 V. The bridge-bonded adsorbed formate band completely disappears at 1.2 V and reappears in the reverse negative-going scan associated with the reduction of the surface oxide, indicating that bridge-bonded formate is not adsorbed on the fully oxidized surface. After reaching to a maximum at ~0.6 V, the bridge-bonded adsorbed formate band decreases its intensity at less positive potentials. The bands of CO_L and CO_B reappear at around 0.3 V and grow at lower potentials.

We carried out the same experiments in buffered solutions with higher pHs and observed that the bridge-bonded formate band becomes weaker with increasing pH from ~4 and completely disappears at pH ~6. A representative set of spectra of the electrode surface at pH 6.8 are shown in Fig. 3a. The absence of bridge-bonded formate in neutral media is well correlated with the decrease in HCOOH concentration (see the blue dashed trace in Fig. 1b), implying that bridge-bonded adsorbed formate is formed only from HCOOH. If bridge-bonded adsorbed formate were quickly decomposed to CO_2, its coverage could be smaller. However, a similar result was obtained for the adsorption of acetic acid/acetate (pKa = 4.75) that is not oxidized at all in this potential range, i.e., the symmetric O-C-O stretching vibration of adsorbed acetate was observed only at pH < 6 (data not shown). Therefore, the absence of bridge-bonded adsorbed formate in the neutral solution is not due to its rapid oxidation. The strong band around 1130 cm^{-1} in the spectra that appears after the oxidative removal of CO_{ads} is assigned to a P–O stretching mode of a phosphate anion adsorbed on the electrode surface (HPO_4^- [44]). In the negative-going scan, a very weak band assigned to either carbonate [46] or bicarbonate [47] derived from CO_2 is observed around 1450 cm^{-1}. No other adsorbed spieces are observed in the SEIRA spectra.

The CV recorded simultaneously with the SEIRA spectra is shown in Fig. 3b (top panel) together with the potential dependence of the integrated band intensities of CO_L and CO_B taken from the spectra in Fig. 3a (bottom panel). The CV is simpler than that at pH 1.5 and only one anodic peak is observed in the both positive- and negative-going scans at different potentials. If the CV is plotted against the reversible hydrogen electrode (RHE), the peaks in the positive- and negative-going scans correspond to peak p1 and peak p5 observed in the CV at pH 1.5 (Fig. 2b, bottom panel), respectively. On the other hand, anodic peaks corresponding to peak p_2, peak p_3, and peak p_4 are absent, which suggests that bridge-bonded adsorbed formate is responsible for the appearance of these three anodic peaks. Another notable difference is the potential dependence of the band intensity of CO_L in the positive-going scan. It is weak at the beginning of the potential scan and grows in between −0.3 and 0 V. In the negative-going scan, CO_{ads} starts to be formed at 0 V and saturates at ~ −0.3 V, indicating that CO_{ads} is formed in the limited potential range.

The voltammetric features of $HCOO^-$ oxidation in alkaline media are different from those in neutral media. A representative CV at pH 11.7 is shown in Fig. 4a (top panel). Two anodic peaks and one peak are observed in the positive- and negative-going scans, respectively. The second anodic peak at -0.05 V in the positive-going scan and the peak at -0.33 V in the negative-going scan correspond to peak p1 and peak p5 in Figs. 2 and 3 (on the RHE scale). On the other hand, the first anodic peak at −0.35 V in the positive-going scan, labeled as p0, has no counterpart at pH 1.5 and 6.8. Peak p0 and peak p5 occur at almost the same potentials and their peak currents are almost the same, indicating that the same reaction takes place at both peak p0 and peak p5. Since the peak currents of peak p0 and peak p5 were proportional to the concentration of $HCOO^-$ added into the solution, these peaks are ascribed to $HCOO^-$ oxidation. The appearance of the anodic peaks at the same potential in the both positive- and negative-going scans is due to the low CO coverage, which is confirmed by the

weak integrated band intensities of CO_L and CO_B as shown in the same figure (lower panel): the maximum intensity of CO_L is only 20% of that observed in acidic media (saturated CO coverage), while the intensity of the CO_B band is comparable to that in acidic and neutral media.

Stripping voltammetry by John et al. [27] revealed that two strongly adsorbed species are formed from $HCOO^-$ at low potentials and exhibit two oxidative stripping peaks at peak p0 and peak p1 (in the present notation of peaks). The authors ascribed the stripping peaks to the oxidation of an intermediate of $HCOO^-$ oxidation (termed as X1) and of CO_{ads} (termed as X2), respectively. However, the infrared data shown above indicates that CO_L and CO_B are oxidized selectively at peak p0 and at peak p1, respectively. Other adsorbates detected by SEIRAS were (bi)carbonate and phosphate anion, and no infrared absorption bands that could be ascribed to the intermediate X1 were detected (the spectra are not shown because the spectral features were similar to those in Fig. 3a). Accordingly, we assign X1 and X2 to CO_L and CO_B, respectively. The peak current of peak p1 was independent of concentration of $HCOO^-$, indicating that peak p1 arises only from the oxidation of CO_B.

The results of the spectroelectrochemical measurements are summarized in a Pourbaix-type diagram (*E* vs. pH diagram) shown in Fig. 5. Blue symbols represent the peak potentials of peak p3, peak p4, and peak p5 at pH 1.5, and peak 5 at pH > 6. The results in the pH range between 3 and 5, where the oxidation current is large (Fig. 1), were omitted in the diagram because the voltammetric features in the negative-going scan were seriously distorted by the ohmic drop, which arose from the large real surface area of the thin film electrode (~10 cm^2 determined from the charge under the hydrogen desorption peaks) and a relatively large cell resistance of ~10 Ω (mostly due to the resistance of the thin film electrode). Instead, the peak potentials of the anodic peak, E_p, observed with a rotating Pt disc electrode (5 mm in diameter) in the same buffered solutions containing 50 mM $HCOOH/HCOO^-$ (Fig. 1b)

recorded in the negative-going scan are shown by black symbols (the result reported in ref. 35). In this case, only a single oxidation peak was observed at pH < 5. The peak shifted to lower potentials with increasing pH at a rate of 60 mV per pH and a shoulder appeared at around pH 5.5. At higher pHs, the higher potential component of the anodic peak disappeared and the lower potential component shifted to the lower potentials accompanying by the decrease in peak current. The peak potentials in the two independent measurements are in good agreement at pH > 6. Red symbols represent the potential at which the IR band of CO_{ads} appeared in the negative-going scan. The onset potential of CO_{ads} formation is independent of pH at pH < ~5 and negatively shifted at pH > ~5 at a rate of 60 mV per pH. Additionally shown are the surface oxidation and upd hydrogen adsorption (H_{upd}) regions, which were determined in the positive- and negative-going scans, respectively, in the supporting electrolyte solutions free of $HCOOH/HCOO^-$ (experimental data points were omitted to avoid complexity). The white area is the double-layer region, but it is noted that some amount of surface oxide or OH_{ads} remains in this region in the negative-going scan during which the IR and electrochemical data were collected due to the relatively slow kinetics of the reduction of surface oxide (see dotted CVs in Figs. 2, 3, and 4 recorded in HCOONa-free electrolyte solutions). Finally, green symbols represent the potentials at which the band of adsorbed phosphate appeared in the positive-going scan in the $HCOOH/HCOO^-$-free solutions. This data could be a rough measure of the onset potential of the adsorption of anionic species, including $HCOO^-$ and OH^-. In fact, the onset of OH^- adsorption is reported to be located in the H_{upd} region [48, 49].

The Pourbaix diagram highlights two interesting features of $HCOOH/HCOO^-$ oxidation and CO_{ads} formation. One is that E_p is located in the double layer region at pH < 5.5 and jumps to the onset potential of hydrogen adsorption at pH > 5.5. The other is that the onset of CO_{ads} formation is independent of pH at pH < 5.5, whereas it depends on pH at pH >

5.5 and is located at the onset potential of H_{upd}. Remembering that bridge-bonded formate is adsorbed on the electrode surface at pH < 6, the different pH dependences of E_p and CO_{ads} formation at pH < 5.5 and > 5.5 will be related to the presence and absence of bridge-bonded adsorbed formate rather than to the acid-base equilibrium of HCOOH in the solution (pK_a = 3.75). In fact, Cuesta et al. [16, 18] showed that CO_{ads} is formed in acidic media by the reduction of bridge-bonded adsorbed formate ($HCOO_{ads} + H^+ + e^- \rightarrow CO_{ads} + H_2O$). The rate of the reaction depends on potential [16, 18, 50] and pH, but the onset potential is independent of pH. The pH-independence could also be explained by the pure chemical dehydration of HCOOH ($HCOOH \rightarrow CO_{ads} + H_2O$), but this mechanism is not suitable since θ_{CO} increases as the potential is made more negative (Fig. 2), i.e., CO_{ads} formation is an electrochemical reduction process. On the other hand, the source of CO_{ads} must be $HCOO^-$ in alkaline media. As shown in Figs. 3 and 4, CO_{ads} accumulation occurs in a limited potential range locating in between the red and green lines in Fig. 5, i.e., in the potential range where both $HCOO^-$ and H_{upd} can be coadsorbed. Therefore, CO_{ads} is likely to be formed by a reaction of adsorbed $HCOO^-$ with H_{upd} although we did not observe the adsorbed $HCOO^-$ by SEIRAS. Since $HCOO^-$ competes with OH_{ads} for free sites, CO_{ads} accumulation is slow in alkaline media compared with that in acid [27], which is supported by the IR data shown above.

3.2 Kinetic modeling of HCOOH/$HCOO^-$ oxidation

As shown in Fig. 1, peak current (j_p) of the HCOOH/$HCOO^-$ oxidation in the negative-going scan shows a volcano-shaped pH dependence peaked at pH ~ 4. Since the HCOOH concentration decreases with pH, the increase of j_p at pH < 4 apparently cannot be explained by the direct HCOOH mechanism which assumes HCOOH oxidation via a weakly adsorbed HCOOH precursor. Bridge-bonded adsorbed formate mechanism also is not compatible with the result because the coverage of bridge-bonded adsorbed formate was

almost constant at pH < 4. Rather, the result strongly suggests that $HCOO^-$ is more reactive than HCOOH and its oxidation contributes dominantly to the anodic current. However, if it is so, why does the anodic current decrease at pH > 5 despite the further increase of $HCOO^-$ concentration? Grozovski et al. [22] explained the small anodic current in alkaline media to the absence of adsorbed formate on the electrode surface. On the other hand, John et al. [27] proposed that $HCOO^-$ is adsorbed on the electrode so strongly that its oxidation is very slow. However, both proposals do not account for the very high activity of $HCOO^-$ at pHs around 4.

For being oxidized (electro)catalytically, $HCOO^-$ must be adsorbed on the electrode surface, but no infrared absorption bands corresponding to adsorbed $HCOO^-$ were detected in neutral and alkaline media as described above. Therefore, it will be reasonable to assume that $HCOO^-$ is oxidized directly as

$$HCOO^- \rightarrow CO_2 + H^+ + 2e^- \quad (1)$$

via transiently adsorbed $HCOO^-$ and that its adsorption is significantly suppressed in alkaline media. A possible origin of the suppression of $HCOO^-$ adsorption or oxidation is the oxidation of the electrode surface or adsorption of hydroxyl species (OH_{ads}) [17, 27, 51], the precursor state of surface oxidation [52]. Given that HCOOH/$HCOO^-$ oxidation is kinetically controlled [15, 35], we propose a simple kinetic model that reasonably explains the significant pH dependence of HCOOH/$HCOO^-$ oxidation. The essence of the model is schematically depicted in Fig. 6. Following the Butler-Volmer rate law, the rate constant of $HCOO^-$ oxidation (k_{ox}) should increase exponentially as the potential is made more positive (the blue curve in Fig. 6a). On the other hand, free surface sites available for $HCOO^-$ oxidation are reduced as the potential is made more positive due to the oxidation of the electrode surface. The potential dependence of the coverage of surface oxide (θ_{ox}) may be represented as the black trace. Since the oxidation current is proportional to $k_{ox}(1 - \theta_{ox})$, a peak should appear in

the voltammogram at a potential where $\theta_{ox} \sim 0.5$, as shown by the red curve in the figure. The onset of the surface oxidation shifts negatively as the pH of the solution is increased at a rate of 60 mV per pH, while k_{ox} is independent of pH. Accordingly, the anodic peak shifts negatively and becomes smaller with increasing pH. $k_{ox}(1 - \theta_{ox})$ at the peak potential should decrease exponentially with pH as shown by the purple curve in Fig. 6b. The anodic current also should be proportional to the concentration of $HCOO^-$ ($[HCOO^-]$), which increases as the pH is increased. As a result, the peak current, $j_p = 2F[k_1(1 - \theta_{ox})]_{max}\,[HCOO^-]$, is expected to yield a volcano-type pH dependence peaked at pH ~ pK_a of HCOOH, as shown by the red trace in Fig. 6b. The validity of this idea is substantiated in the following by mathematical modeling of the steady-state voltammogram.

We will model the surface oxidation by a simple reversible reaction represented by

$$H_2O + Pt \leftrightarrows Pt\text{-}OH_{ads} + H^+ + e^- \qquad (2)$$

On a real polycrystalline surface, OH_{ads} is oxidized further and the corresponding reactions are not reversible. However, to model the inhibition of HCOOH/$HCOO^-$ oxidation by Pt surface oxidation, the introduction of one surface oxygen species is sufficient and reaction 2 serves that purpose well [51, 53]. In acidic media, HCOOH is adsorbed on the electrode surface as bridge-bonded formate (b-$HCOO_{ads}$)

$$HCOOH + 2Pt \leftrightarrows b\text{-}HCOO_{ads} + H^+ + e^- \qquad (3)$$

as evidenced by SEIRAS and should suppress the direct oxidation of $HCOO^-$ by blocking active sites. Therefore, bridge-bonded adsorbed formate also must be included in the simulation. Following Samjeské et al. [12-15], bridge-bonded formate is assumed tentatively to be oxidized to CO_2 irreversibly:

$$b\text{-}HCOO_{ads} \rightarrow CO_2 + H^+ + e^- + 2Pt \qquad (4)$$

The reverse reaction has not been observed on Pt. We will assume that the HCOOH/$HCOO^-$ equilibrium is maintained at the interface. Coverages of CO_{ads}, H_{upd}, and adsorbed (bi)carbonate are negligible in the potential range of $HCOO^-$ oxidation as have been shown by SEIRAS. Adsorption of phosphate anions is also neglected for the sake of simplicity because the pH dependence of HCOOH/$HCOO^-$ oxidation in phosphate buffered solutions (Fig. 1) is similar to that observed in $HClO_4/ClO_4^-$ and HSO_4^-/SO_4^{2-} solutions [29-34].

Under such conditions, the coverages of OH_{ads} (θ_{OH}) and bridge-bonded adsorbed formate ($\theta_{b\text{-}f}$) satisfy the following differential equations:

$$\frac{d\theta_{OH}}{dt} = k_2(1-\theta_{b\text{-}f}-\theta_{OH}) - k_{-2}[H^+]\theta_{OH}$$

$$(5)\ \frac{d\theta_{b-f}}{dt} = k_3[HCOOH](1-\theta_{OH}-\theta_{b-f}) - k_{-3}[H^+]\theta_{b-f} - k_4\theta_{b\text{-}f} \qquad (6)$$

where $k_{\pm i}$ (i = 1, 2, 3, and 4) is the rate constant of each reaction at a potential E with plus for the forward reaction (oxidation or adsorption) and minus for the backward reaction (reduction or desorption), and assumed to follow the Butler-Volmer rate law with transfer coefficient α:

$$k_i = k_i^\circ \left[\frac{\alpha n F(E-E_i^\circ)}{RT}\right],\quad k_{-i} = k_{-i}^\circ \exp\left[\frac{-(1-\alpha)nF(E-E_i^\circ)}{RT}\right] \qquad (7)$$

k_i° is the rate constant at the standard equilibrium potential E_i°, n is the number of electrons transferred, and F, R, and T have the usual meanings. For reaction (4), first order, [22] second order [16, 17], and parabolic [12-14] rate equations with respect to $\theta_{b\text{-}f}$ have been proposed, but the first order rate law is assumed here for the sake of simplicity. By applying the steady-state approximation

$$d\theta_{b\text{-}f}/dt = d\theta_{OH}/dt = 0 \qquad (8)$$

θ_{OH} and $\theta_{b\text{-}f}$ are given as

$$\theta_{b\text{-}f} = \left[1+\frac{k_{-3}[H^+]+k_4}{k_3[HCOOH]}\left(1+\frac{1}{K_2}\right)\right]^{-1} \qquad (9)$$

$$\theta_{ox} = (1-\theta_{b\text{-}f})/(1+K_2) \quad (10)$$

where

$$K_2 = \frac{k_{-2}}{k_2}[H^+] = K_2^\circ[H^+]\exp\left\{\frac{-F(E-E_2^\circ)}{RT}\right\} \quad (11)$$

The current density j is given by adding up all contributions from the direct $HCOO^-$ oxidation (1), j_{HCOO-}, and the oxidation of HCOOH via bridge-bonded adsorbed formate (reactions (3) and (4)), $j_{b\text{-formate}}$:

$$j = j_{HCOO^-} + j_{b\text{-formate}} = 2Fk_1(1-\theta_{b\text{-}f}-\theta_{OH})[HCOO^-] + 2Fk_4\theta_{b\text{-}f} \quad (12)$$

In Fig. 7, steady-state voltammograms for [HCOOH/$HCOO^-$] = 0.1 M calculated by using the parameter set shown in the caption are presented. The parameters were chosen to give the maximum of the peak current, j_p, of ~ 5 mA cm^{-2} around pH 4 for [HCOOH/$HCOO^-$] = 50 mM (Fig. 1) and $\theta_{b\text{-}f}$ ~ 0.8 for [HCOOH/$HCOO^-$] = 10 mM [22]. Among the parameters, the most important is k_4, which must be non-zero, i.e., bridge-bonded adsorbed formate must be decomposed to CO_2. Otherwise, the electrode surface is fully covered by bridge-bonded adsorbed formate over a wide potential and pH range and $HCOO^-$ oxidation is seriously suppressed (data not shown). As shown in Fig. 7a, the simulated steady-state voltammogram strongly depends on pH. In accordance with the experiment, the peak current for $HCOO^-$ oxidation, $j_{p,HCOO-}$, increases monotonically with increasing pH up to 4.5 and decreases at higher pHs as shown in Fig. 7b (red trace), while the current carried by the bridge-bonded adsorbed formate pathway ($j_{p,b\text{-formate}}$) is very small over the wide pH range. The observed pH dependence of the adsorption of bridge-bonded formate at pH < 6 also is well reproduced as shown in the colored contour plot in Fig. 7c. (Note that in reality its adsorption is limited in the low potential region due to the accumulation of CO_{ads}).

The model also simulates the negative shift of peak potential E_p with pH but does not reproduce the experiment perfectly. In the simulation, E_p shifts to lower potentials with

increasing pH with a slope of −60 mV per pH except in the pH range between 4 and 6 where the shift is larger (black line in Fig. 7b, the both pathways track the same trace), whereas the peak splits into two at pHs around 5 in the experiment (Fig. 5). The discrepancy may be due to the island formation of bridge-bonded adsorbed formate in the real system, which cannot be simulated by the Langmuir adsorption isotherm used in the simulation (eq. 6). Island formation of bridge-bonded adsorbed formate has been suggested in both UHV[54] and electrochemical environment [55].

As shown above, the decomposition of bridge-bonded adsorbed formate is very slow. Therefore bridge-bonded adsorbed formate blocks active sites and inhibits the direct $HCOO^-$ pathway as shown in Fig. 8, where the simulated pH dependence of peak current with (red curve) and without (blue curve) bridge-bonded adsorbed formate are compared. The simulation gives an answer to a question why Pd, on which bridge-bonded adsorbed formate does not exist, has a higher catalytic activity than Pt for HCOOH oxidation in acidic media [56]. Nevertheless, it should be noted that bridge-bonded adsorbed formate also enhances, albeit indirectly, $HCOO^-$ oxidation. The dotted black straight line in Fig. 7b represents the pH dependence of E_p when bridge-bonded formate is assumed not to be adsorbed as on Pd. A comparison of the E_p curves with and without bridge-bonded adsorbed formate reveals that E_p is positively shifted by bridge-bonded adsorbed formate. The shift (ΔE_p) becomes larger as $\theta_{b\text{-}f}$ increases. Following the Buttler-Volmer rate law, the calculated positive shift of $\Delta E_p \sim$ 0.1 V increases $j_{p,HCOO^-}$ by a factor of 7. The shift amounts to 0.2 V in the experiment (Fig. 5), which increases $j_{p,HCOO^-}$ by a factor of 49. Due to this effect, the suppression of the direct $HCOO^-$ pathway by bridge-bonded adsorbed formate is not fatal despite its large coverage (> 0.95) . The positive shift of E_p is due to the suppression of surface oxidation by bridge-bonded adsorbed formate, as can be seen from the pH dependence of θ_{OH} (light blue contour plot) in Fig. 7c. In fact, the suppression of surface oxidation by bridge-bonded adsorbed formate has

been confirmed experimentally [14]. The E_p-pH curve shown by the pink thick dashed trace is located at the boundary of the bridge-bonded formate and OH adsorption regions (at $\theta_{OH} \approx \theta_{b\text{-}f}$). Since $\theta_{b\text{-}f}$ is less than 1 (i.e., $k_4 \neq 0$), $HCOO^-$ oxidation in the surface oxidation region of Pt (in the blank solution) remain possible on a surface covered by bridge-bonded formate.

A remaining issue is whether HCOOH is directly oxidized. Theoretical studies compared the energetics of the bridge-bonded adsorbed pathway and the direct HCOOH pathway [23-25], but the direct $HCOO^-$ pathway was not considered in the theoretical studies. Regarding this issue, it is worth noting that the direct $HCOO^-$ oxidation gives a considerable current even in acidic media (Figs. 7 and 8) despite its very small concentration (0.018% at pH 0). This means that HCOOH is oxidized after being converted to $HCOO^-$. The direct HCOOH pathway never exceeds the direct $HCOO^-$ pathway, if any: If oxidation current due to direct HCOOH pathway were comparable to or larger than that due to the direct $HCOO^-$ pathway, the monotonic increase of the oxidation current with pH in acidic media (Fig. 1) cannot be explained.

One remarkable result obtained in the present study is that HCOOH/$HCOO^-$ oxidation exhibits an optimal performance at a pH around 4, which is close to the pK_a of HCOOH. A similar trend has been observed also for the oxidation of some alcohols and aldehydes [30]. If bridge-bonded adsorbed formate is assumed to be absent on the electrode, as in the case of HCOOH oxidation on Pd [56], the simulation showed that the maximum of j_p appears exactly at pH = pK_a (Fig. 8). A theoretical thermodynamic argument has shown that this is a generic feature of sequential proton-electron transfer reactions ($AH \leftrightarrows A^- + H^+$ followed by $A^- \rightarrow A + e^-$) [36-38]. Therefore, the pK_a of the molecule of interest is an important factor for predicting the optimal pH for its oxidation.

3.3 Interpretation of multiple oxidation peaks in CV

As shown in Fig. 2b (top panel), HCOOH oxidation in acidic media exhibits two anodic peaks in the positive-going scan (peak p1 and peak p2), while a single oxidation peak is observed with shoulders at both positive and negative side in the negative-going scan (a single peak with a shoulder at the low potential side is observed at higher HCOOH concentrations [6, 13, 14, 51, 57])). The interpretation of the complex voltammetric features has been the subject of discussion, because the origins of the two anodic peaks in the positive-going scan are the key issues for understanding electrochemical oscillations observed during HCOOH oxidation [51, 53, 58, 59].

The two oxidation peaks in the positive-going scan are often interpreted in terms of two different reactions at different potentials [6, 60]. However, such an explanation will not be reasonable because HCOOH oxidation after being converted to $HCOO^-$ is the major reaction route in acidic media and the contribution of CO pathway to the total current is negligible [13, 19, 20]. Breiter [61] postulated that the first anodic peak is due to oxidation of HCOOH to CO_2 on the small fraction of the surface which was not blocked by adsorbed intermediates. Oxidation of these intermediates at more positive potentials uncovers a large number of active sites on which further oxidation of HCOOH can take place, thus causing the rise in current leading to the second anodic peak. A similar explanation was made also by Strasser et al.[51]. On the other hand, Okamoto and Tanaka [62] proposed that H_2O adsorbed at free sites suppresses CO_{ads} oxidation to yield the negative differential resistance (NDR) at the positive side of peak p1 and the replacement of adsorbed H_2O by OH_{ads} facilitates CO_{ads} oxidation at higher potentials leading to the second peak. The role of CO_{ads} in these explanations is well supported by SEIRAS (Fig. 2). However, these earlier explanations are insufficient because the adsorption of bridge-bonded formate on the electrode surface was not included (which was not known before the SEIRAS study by Miki et al. in 2002 [9]). Samjeské et al. [12, 13] explained the NDR and the second anodic peak by assuming that

bridge-bonded adsorbed formate is decomposed to CO_2 and that its reaction rate is a strong function of the coverage of free sites. However, this explanation conflicts with the conclusion in the present study that the decomposition of bridge-bonded adsorbed formate is very slow and HCOOH oxidation via $HCOO^-$ is the major reaction pathway.

Here we will provide a new interpretation on the basis on the following experimental results: (i) when neither CO_{ads} nor bridge-bonded adsorbed formate exist on the surface (or when θ_{CO} is small), $HCOO^-$ oxidation yields a single anodic peak which appears at a same low potential in both the positive- and negative-going scan (Fig. 4), (ii) in the presence of CO_{ads}, the anodic peak in the positive-going scan is shifted positively to a potential at which CO_{ads} is oxidized (Fig. 3), and (iii) the second anodic peak appears only when bridge-bonded formate is coadsorbed with CO (Fig. 2). In the latter case, CO_{ads} is not essential because a similar CV is observed also on Au, where bridge-bonded formate is adsorbed but CO_{ads} is absent [17]. The results clearly indicate that bridge-bonded adsorbed formate is responsible for the second peak. Since bridge-bonded adsorbed formate enables $HCOO^-$ oxidation at high potentials by suppressing the oxidation of the electrode surface as mentioned before, the second peak appears in the surface oxidation region.

The multiple anodic peaks in the negative-going scan also can be ascribed to bridge-bonded adsorbed formate as has been suggested before. Since bridge-bonded adsorbed formate is likely to form islands, $HCOO^-$ oxidation in the island occurs at higher potential than in the regions free of bridge-bonded adsorbed formate to yield multiple anodic peaks in the voltammogram.

5. Conclusion and remarks

The examination of the electrooxidation of HCOOH/$HCOO^-$ on Pt over a wide range of solution pH revealed that the oxidation current exhibits a volcano-shaped pH dependence

peaked at a pH close to the pK_a of HCOOH (3.75). A simple mathematical modeling of the reaction revealed that the main reaction route is the oxidation of $HCOO^-$ over the whole pH range and that HCOOH is oxidized after being converted to $HCOO^-$ via the acid-base equilibrium ($HCOOH \leftrightarrows HCOO^- + H^+$). The ascending part at pH < pK_a is ascribed mainly to the increase of the molar ratio of $HCOO^-$, while the descending part at pH > pK_a is ascribed to the suppression of $HCOO^-$ oxidation by adsorbed OH and/or surface oxidation. The SEIRAS revealed that HCOOH is adsorbed on Pt as bridge-bonded adsorbed formate at pH < ~5. The bridge-bonded adsorbed formate blocks active sites for $HCOO^-$ oxidation but enhances $HCOO^-$ oxidation at high potentials by preventing the adsorption of OH and oxidation of the electrode surface. CO_{ads} is formed by the reduction of bridge-bonded adsorbed formate at pH < ~ 5 and presumably by a reaction of transiently adsorbed $HCOO^-$ and H_{ads} at pH > ~5. The mechanistic model presented in this work also well explains the complex CVs of HCOOH oxidation in acidic media.

In earlier studies, the reaction mechanism of HCOOH oxidation (bridge-bonded adsorbed formate and direct HCOOH pathways) has been discussed on the basis of the relation between oxidation current and the coverage of bridge-bonded adsorbed formate. However, the main reaction route is the direct $HCOO^-$ pathway that was not considered in previous studies. Accordingly, such an approach to identify the reaction mechanism will not be fruitful, and could even be misleading. The situation is the same in previous theoretical studies, where no attention was paid to $HCOO^-$ oxidation.

The most important finding in the present study is that the best performance can be achieved at pH ≈ pK_a. This is a general property in catalytic proton-coupled electron transfer reactions. In this point of view, it can be inferred that most DFAFCs using cation- and anion-exchange membranes are not operated under the optimal conditions. If pH in the membranes could be less than –6, however, higher performance is expected from the mathematical

simulation shown in the present work due to the activation of bridge-bonded adsorbed formate pathway. In this case, direct HCOOH pathway also could be activated.

Acknowledgements

This work was supported by Japanese Society for the Promotion of Science (JSPS) KAKENHI Grant Number 24550143 and 24750117. MTMK gratefully acknowledges the award of Long-Term Fellowship of JSPS (No. L-11527) and Visiting Professorship of Hokkaido University. TU acknowledges Grants-in-Aid for Regional R&D Proposal-Based Program from Northern Advancement Center for Science & Technology of Hokkaido, Japan, and MEXT Project of Integrated Research on Chemical Synthesis. JJ acknowledges scholarship of Asian Graduate School, Hokkaido University.

References

[1] L. Carrette, K.A. Friedrich, U. Stimming, Fuel cells: Principles, types, fuels, and applications, ChemPhysChem, 1 (2000) 162.
[2] C. Rice, S. Ha, R.I. Masel, P. Waszczuk, A. Wieckowski, T. Barnard, Direct formic acid fuel cells, J. Power Sources, 111 (2002) 83.
[3] U.B. Demirci, Direct liquid-feed fuel cells: Thermodynamic and environmental concerns, J. Power Sources, 169 (2007) 239.
[4] S. Uhm, H.J. Lee, J. Lee, Understanding underlying processes in formic acid fuel cells, Phys. Chem. Chem. Phys., 11 (2009) 9326.
[5] A. Capon, R. Parsons, Oxidation of formic-acid at noble-metal electrodes: I. Review of previous work, J. Electroanal. Chem., 44 (1973) 1.
[6] A. Capon, R. Parsons, Oxidation of formic-acid on noble-metal electrodes: II. Comparison of behavior of pure electrodes, J. Electroanal. Chem., 44 (1973) 239.
[7] A. Capon, R. Parsons, Oxidation of formic-acid at noble-metal electrodes Part III. Intermediates and mechanism on platinum-electrodes, J. Electroanal. Chem., 45 (1973) 205.
[8] K. Kunimatsu, Infrared spectroscopic study of methanol and formic acid adsorbates on a platinum electrode: Part 1. Comparison of the infrared absorption intensities of linear CO(a) derived from CO, CH_3OH and HCOOH, J. Electroanal. Chem., 213 (1986) 149.
[9] A. Miki, S. Ye, M. Osawa, Surface-enhanced IR absorption on platinum nanoparticles: An application to real-time monitoring of electrocatalytic reactions, Chem. Commun., (2002) 1500.
[10] M. Osawa, Dynamic processes in electrochemical reactions studied by surface-enhanced infrared absorption spectroscopy (SEIRAS), Bull. Chem. Soc. Jpn., 70 (1997) 2861.

[11] M. Osawa, In-situ surface-enhanced infrared spectorscopy of the electrode/solution interface, in: R.C. Alkire, D.M. Kolb, J. Lipkowski, P.H. Ross (Eds.) Diffraction and Spectroscopic Methods in Electrochemistry (Advances in Electrochemical Science and Enginnering, vol. 9), Wiley-VCH, Weinheim, 2006, pp. Chapter 8.
[12] G. Samjeské, M. Osawa, Current oscillations during formic acid oxidation on a Pt electrode: Insight into the mechanism by time-resolved IR spectroscopy, Angew. Chem. Int. Ed., 44 (2005) 5694.
[13] G. Samjeské, A. Miki, S. Ye, A. Yamakata, Y. Mukouyama, H. Okamoto, M. Osawa, Potential oscillations in galvanostatic electrooxidation of formic acid on platinum: A time-resolved surface-enhanced infrared study, J. Phys. Chem. B, 109 (2005) 23509.
[14] G. Samjeské, A. Miki, S. Ye, M. Osawa, Mechanistic study of electrocatalytic oxidation of formic acid at platinum in acidic solution by time-resolved surface-enhanced infrared absorption spectroscopy, J. Phys. Chem. C, 110 (2006) 16559.
[15] M. Osawa, K. Komatsu, G. Samjeské, T. Uchida, T. Ikeshoji, A. Cuesta, C. Gutiérrez, The role of bridge-bonded adsorbed formate in the electrocatalytic oxidation of formic acid on platinum, Angew. Chem. Int. Ed., 50 (2011) 1159.
[16] A. Cuesta, G. Cabello, M. Osawa, C. Gutiérrez, Mechanism of the electrocatalytic oxidation of formic acid on metals, ACS Catalysis, 2 (2012) 728.
[17] A. Cuesta, G. Cabello, F.W. Hartl, M. Escudero-Escribano, C. Vaz-Dominguez, L.A. Kibler, M. Osawa, C. Gutiérrez, Electrooxidation of formic acid on gold: An ATR-SEIRAS study of the role of adsorbed formate, Catal. Today, 202 (2013) 79.
[18] A. Cuesta, G. Cabello, C. Gutiérrez, M. Osawa, Adsorbed formate: The key intermediate in the oxidation of formic acid on platinum electrodes, Phys. Chem. Chem. Phys., 13 (2011) 20091.
[19] Y.X. Chen, M. Heinen, Z. Jusys, R.J. Behm, Kinetics and mechanism of the electrooxidation of formic acid – Spectroelectrochemical studies in a flow cell, Angew. Chem. Int. Ed., 45 (2006) 981.
[20] Y.X. Chen, M. Heinen, Z. Jusys, R.J. Behm, Bridge-bonded formate: Active intermediate or spectator species in formic acid oxidation on a Pt film electrode?, Langmuir, 22 (2006) 10399.
[21] Y.X. Chen, M. Heinen, Z. Jusys, R.J. Behm, Kinetic isotope effects in complex reaction networks: Formic acid electro-oxidation, ChemPhysChem, 8 (2007) 380.
[22] V. Grozovski, F.J. Vidal-Iglesias, E. Herrero, J.M. Feliu, Adsorption of formate and its role as intermediate in formic acid oxidation on platinum electrodes, ChemPhysChem, 12 (2011) 1641.
[23] M. Neurock, M. Janik, A. Wieckowski, A first principles comparison of the mechanism and site requirements for the electrocatalytic oxidation of methanol and formic acid over Pt, Faraday Discus., 140 (2008) 363.

[24] H.F. Wang, Z.P. Liu, Formic acid oxidation at Pt/H_2O interface from periodic dft calculations integrated with a continuum solvation model, J. Phys. Chem. C, 113 (2009) 17502.
[25] W. Gao, J.A. Keith, J. Anton, T. Jacob, Theoretical elucidation of the competitive electro-oxidation mechanisms of formic acid on Pt(111), J. Am. Chem. Soc., 132 (2010) 18377.
[26] W.M. Haynes, CRC Handbook of Chemistry and Physics, 92nd edition, 2011-2012.
[27] J. John, H.S. Wang, E.D. Rus, H.D. Abruna, Mechanistic studies of formate oxidation on platinum in alkaline medium, J. Phys. Chem. C, 116 (2012) 5810.
[28] J.H. Jiang, J. Scott, A. Wieckowski, Direct evidence of a triple-path mechanism of formate electrooxidation on Pt black in alkaline media at varying temperature. Part I: The electrochemical studies, Electrochim. Acta, 104 (2013) 124.
[29] R.P. Buck, L.R. Griffith, Voltammetric and chronopotentiometric study of the anodic oxidation of methanol, formaldehyde, and formic acid, J. Electrochem. Soc., 109 (1962) 1005.
[30] V.S. Bagotzky, Y.B. Vasilieyev, Some characterization of oxidation reactions of organic compounds on platinum electrodes, Electrochim. Acta, 9 (1964) 869.
[31] B. Beden, C. Lamy, J.M. Leger, Electrocatalytic activity of noble-metals for the oxidation of formate in neutral medium, J. Electroanal. Chem., 101 (1979) 127.
[32] R.R. Adzic, M.I. Hofman, D.M. Drazic, Oxidation of formates on a platinum-electrode in neutral solutions, J. Electroanal. Chem., 110 (1980) 361.
[33] H. Kita, T. Katagiri, K. Kunimatsu, Electrochemical oxidation of HCOONa on Pt in acidic solutions, J. Electroanal. Chem., 220 (1987) 125.
[34] J.L. Haan, R.I. Masel, The influence of solution pH on rates of an electrocatalytic reaction: Formic acid electrooxidation on platinum and palladium, Electrochim. Acta, 54 (2009) 4073.
[35] J. Joo, T. Uchida, A. Cuesta, M.T.M. Koper, M. Osawa, Importance of acid-base equilibrium in electrocatalytic oxidation of formic acid on platinum, J. Am. Chem. Soc., 135 (2013) 9991.
[36] M.T.M. Koper, Thermodynamic theory of multi-electron transfer reactions: Implications for electrocatalysis, J. Electroanal. Chem., 660 (2011) 254.
[37] M.T.M. Koper, Theory of the transition from sequential to concerted electrochemical proton-electron transfer, Phys. Chem. Chem. Phys., (2013).
[38] M.T.M. Koper, Theory of multiple proton-electron transfer reactions and its implications for electrocatalysis, Chem. Sci., 4 (2013) 2710.
[39] Y. Kwon, S.C.S. Lai, P. Rodriguez, M.T.M. Koper, Electrocatalytic oxidation of alcohols on gold in alkaline media: Base or gold catalysis?, J. Am. Chem. Soc., 133 (2011) 6914.

[40] K. Ataka, T. Yotsuyanagi, M. Osawa, Potential-dependent reorientation of water molecules at an electrode/electrolyte interface studied by surface-enhanced infrared absorption spectroscopy, J. Phys. Chem., 100 (1996) 10664.
[41] A. Miki, S. Ye, T. Senzaki, M. Osawa, Surface-enhanced infrared study of catalytic electrooxidation of formaldehyde, methyl formate and dimethoxymethane on platinum electrodes in acid solution, J. Electroanal. Chem., 563 (2004) 23.
[42] M. Osawa, M. Tsushima, H. Mogami, G. Samjeské, A. Yamakata, Structure of water at the electrified platinum-water interface: A study by surface-enhanced infrared absorption spectroscopy, J. Phys. Chem. C, 112 (2008) 4248.
[43] M. Osawa, K. Ataka, K. Yoshii, Y. Nishikawa, Surface-enhanced infrared spectroscopy: The origin of the absorption enhancement and band selection rule in the infrared spectra of molecules adsorbed on fine metal particles, Appl. Spectrosc., 47 (1993) 1497.
[44] R. Gisbert, G. Garcia, M.T.M. Koper, Adsorption of phosphate species on poly-oriented Pt and Pt(111) electrodes over a wide range of pH, Electrochim. Acta, 55 (2010) 7961.
[45] G. Samjeské, K. Komatsu, M. Osawa, Dynamics of CO oxidation on a polycrystalline platinum electrode: A time-resolved infrared study, J. Phys. Chem. C, 113 (2009) 10222.
[46] T. Iwasita, A. Rodes, E. Pastor, Vibrational spectroscopy of carbonate adsorbed on Pt(111) and Pt(110) single-crystal electrodes, J. Electroanal. Chem., 383 (1995) 181.
[47] A. Berna, A. Rodes, J.M. Feliu, F. Illas, A. Gil, A. Clotet, J.M. Ricart, Structural and spectroelectrochemical study of carbonate and bicarbonate adsorbed on Pt(111) and Pd/Pt(111) electrodes, J. Phys. Chem. B, 108 (2004) 17928.
[48] N.M. Markovic, H.A. Gasteiger, N. Philip, Oxygen reduction on platinum low-index single-crystal surfaces in alkaline solution: Rotating ring disk(Pt(hkl)) studies, J. Phys. Chem., 100 (1996) 6715.
[49] M. van der Niet, N. Garcia-Araez, J. Hernandez, J.M. Feliu, M.T.M. Koper, Water dissociation on well-defined platinum surfaces: The electrochemical perspective, Catal. Today, 202 (2013) 105.
[50] V. Grozovski, V. Climent, E. Herrero, J.M. Feliu, Intrinsic activity and poisoning rate for HCOOH oxidation at Pt(100) and vicinal surfaces containing monoatomic (111) steps, ChemPhysChem, 10 (2009) 1922.
[51] P. Strasser, M. Lubke, F. Raspel, M. Eiswirth, G. Ertl, Oscillatory instabilities during formic acid oxidation on Pt(100), Pt(110) and Pt(111) under potentiostatic control. I. Experimental, J. Chem. Phys., 107 (1997) 979.
[52] H. Angerstein-Kozlowska, B.E. Conway, W.B.A. Sharp, The real condition of electrochemically oxidezed platinum surfaces: Part I. Resolution of component processes, J. Electroanal. Chem., 43 (1973) 9.

[53] P. Strasser, M. Eiswirth, G. Ertl, Oscillatory instabilities during formic acid oxidation on Pt(100), Pt(110) and Pt(111) under potentiostatic control. II. Model calculations, J. Chem. Phys., 107 (1997) 991.
[54] R.G. Sharpe, M. Bowker, Kinetic models of surface explosions, J. Phys.: Condens. Matter, 7 (1995) 6379.
[55] J. Wojtowic, N. Marincic, B.E. Conway, Oscillatory kinetics in electrochemical oxidation of formate and ethylene, J. Chem. Phys., 48 (1968) 4333.
[56] H. Miyake, T. Okada, G. Samjeské, M. Osawa, Formic acid electrooxidation on pd in acidic solutions studied by surface-enhanced infrared absorption spectroscopy, Phys. Chem. Chem. Phys., 10 (2008) 3662.
[57] H. Okamoto, W. Kon, Y. Mukouyama, Five current peaks in voltammograms for oxidations of formic acid, formaldehyde, and methanol on platinum, J. Phys. Chem. B, 109 (2005) 15659.
[58] M.T.M. Koper, Oscillations and complex dynamical bifurcation in electrochemical systems, in: I. Prigogine, S.A. Rice (Eds.) Adv. Chem. Phys., vol. 92, John Wiley & Sons, New York, 1996, pp. 161.
[59] H. Okamoto, Mechanistic studies of the potential oscillation and induction period in the oxidation of formic-acid on platinum, Electrochim. Acta, 37 (1992) 37.
[60] W. Gao, J.E. Mueller, Q. Jiang, T. Jacob, The role of CO-adsorbed CO and OH in the electrooxidation of formic acid on Pt(111), Angew. Chem. Int. Ed., 51 (2012) 9448.
[61] M.W. Breiter, Electrochemical Processes in Fuel Cells, Springer-Verlag, New York, 1969.
[62] H. Okamoto, N. Tanaka, Potential oscillation mechanism for formaldehyde oxidation on platinum, Electrochim. Acta, 38 (1993) 503.

Figures

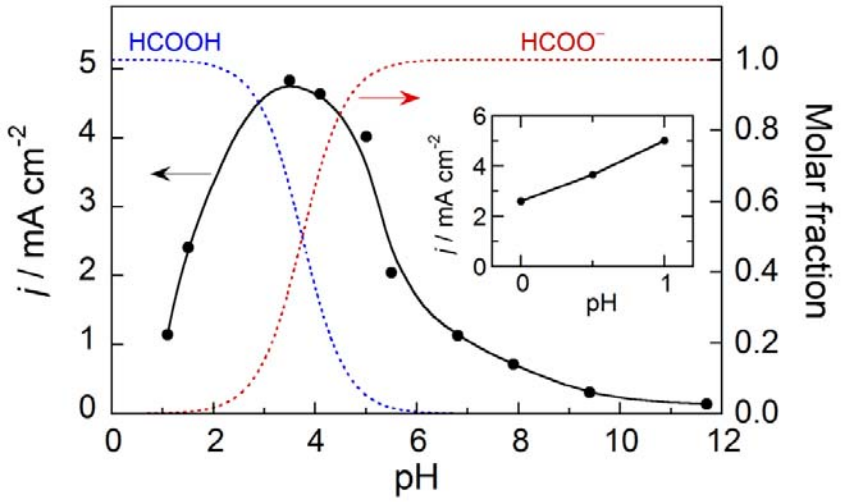

Fig. 1. The pH dependence of the peak current density (j_p) for HCOOH/$HCOO^-$ oxidation on a Pt electrode in phosphate buffered solutions (adopted from Ref. 35). Blue and red dotted traces represent the molar fractions of HCOOH and $HCOO^-$, respectively, in the bulk solution. Solid curves are only a guide to the eye. Inset shows j_p examined in 0.1–1 M $HClO_4$. Owing to the weaker adsorption of ClO_4^-, j_p is larger than in phosphate solutions.

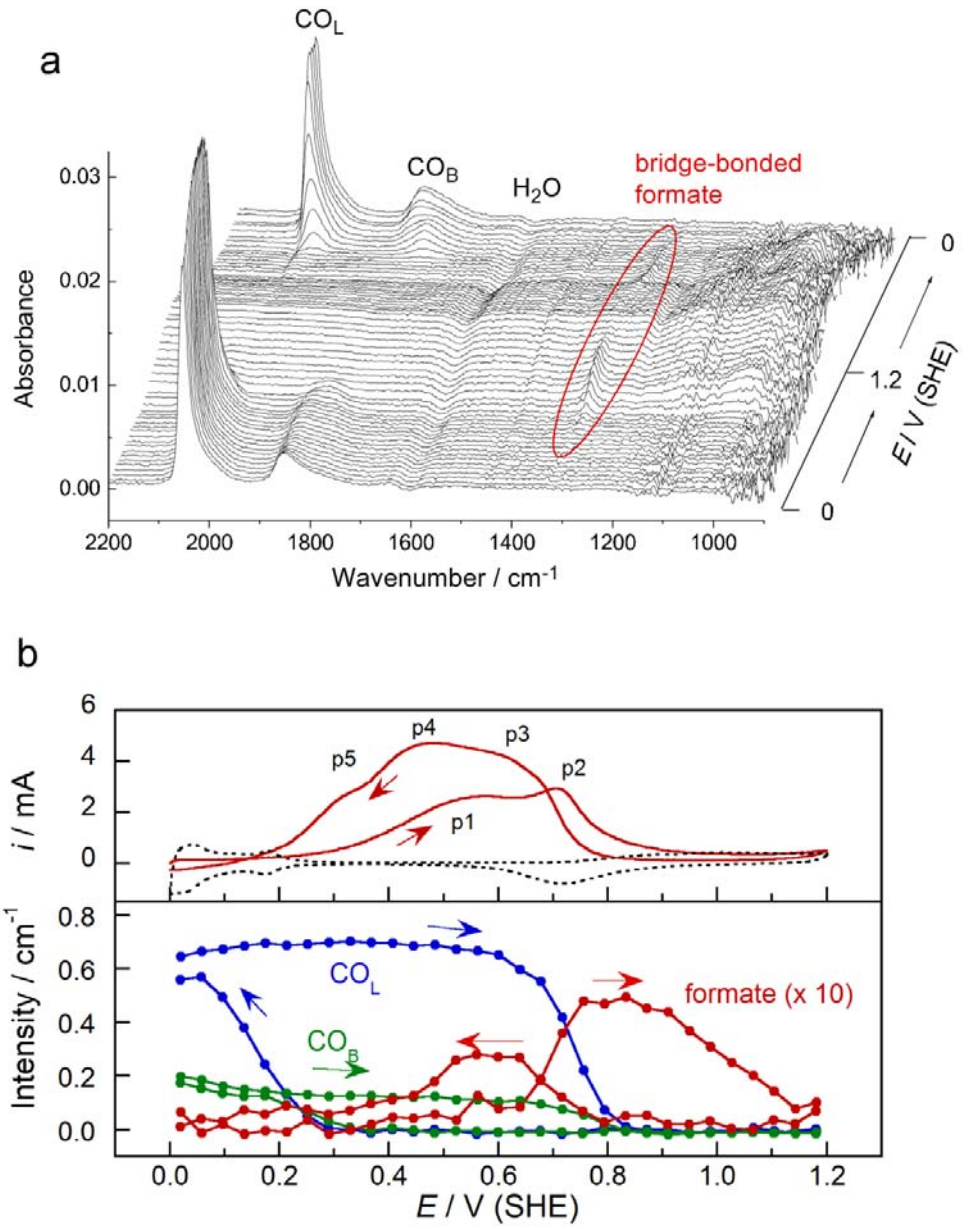

Fig. 2. (a) SEIRA spectra of the surface of a Pt thin-film electrode collected during a potential sweep from 0 to 1.2 and back to 0 V at 20 mV s^{-1} in 0.2 M H_3PO_4 (pH 1.5) containing 20 mM HCOONa. (b) CV recorded simultaneously with the SEIRA spectra (top) and potential dependence of the integrated intensities of the CO_L, CO_B, and bridge-bonded adsorbed formate bands (bottom) obtained from the spectra in (a). The dashed trace is the CV of the electrode in the same electrolyte solution without HCOONa.

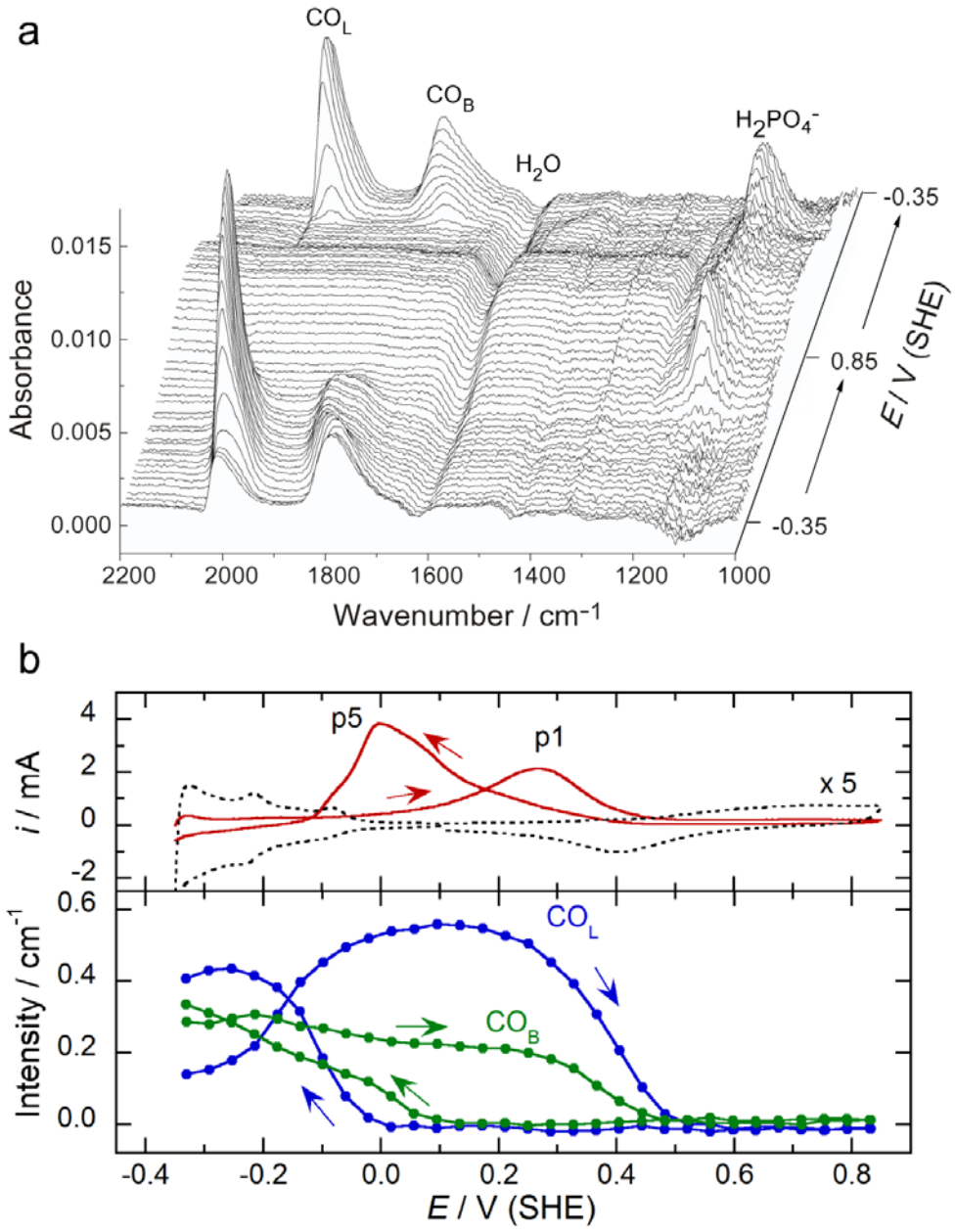

Fig. 3. (a) SEIRA spectra of the surface of a Pt thin-film electrode collected during a potential sweep from −0.3 to 0.9 and back to −0.3 V at 20 mV s^{-1} in 0.2 M phosphate buffer solution of pH 6.8 containing 20 mM HCOONa. (b) CV recorded simultaneously with the SEIRA spectra (top panel) and integrated intensities of the CO_L and CO_B bands in (a) plotted as a function of applied potential (bottom). The dashed trace in the upper panel is the CV in the same electrolyte without HCOONa.

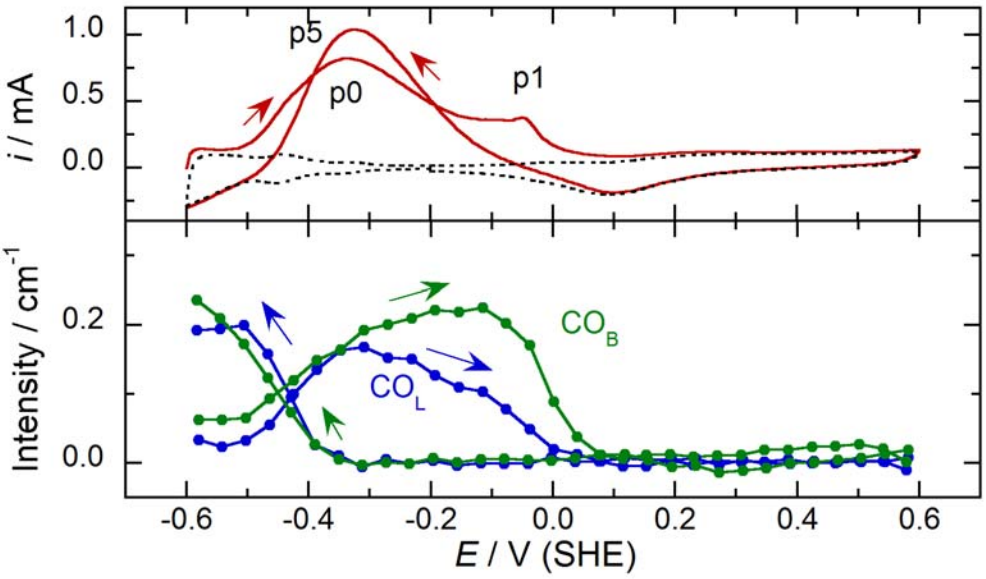

Fig. 4. CV of a Pt thin-film electrode in 0.2 M phosphate buffer solution with pH 11.7 containing 20 mM HCOONa (top panel) at 20 mV s^{-1} (upper panel) and potential dependence of the integrated intensities of the CO_L and CO_B bands taken from SEIRA spectra collected simultaneously with the CV (bottom panel). The dashed trace in the upper panel is the CV in the same electrolyte solution without HCOONa.

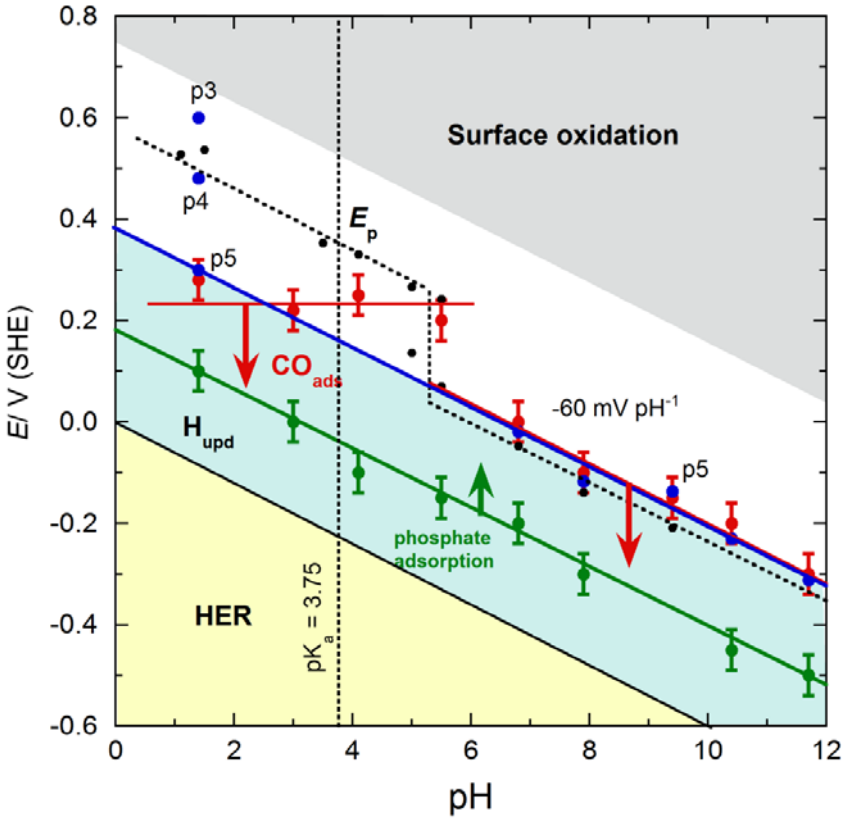

Fig. 5. Pourbaix diagram of the HCOOH/HCOO$^-$ oxidation on Pt. Black symbols: peak potential of the anodic peak, E_p, taken from Ref. 35 ; blue symbols: peak potentials of the anodic peaks or shoulders in the negative-going scan; red symbols: onset potential of CO_{ads} formation in the negative-going sweep; green symbols: onset potential of the adsorption of phosphate anions in the positive-going scan. See further details in the text.

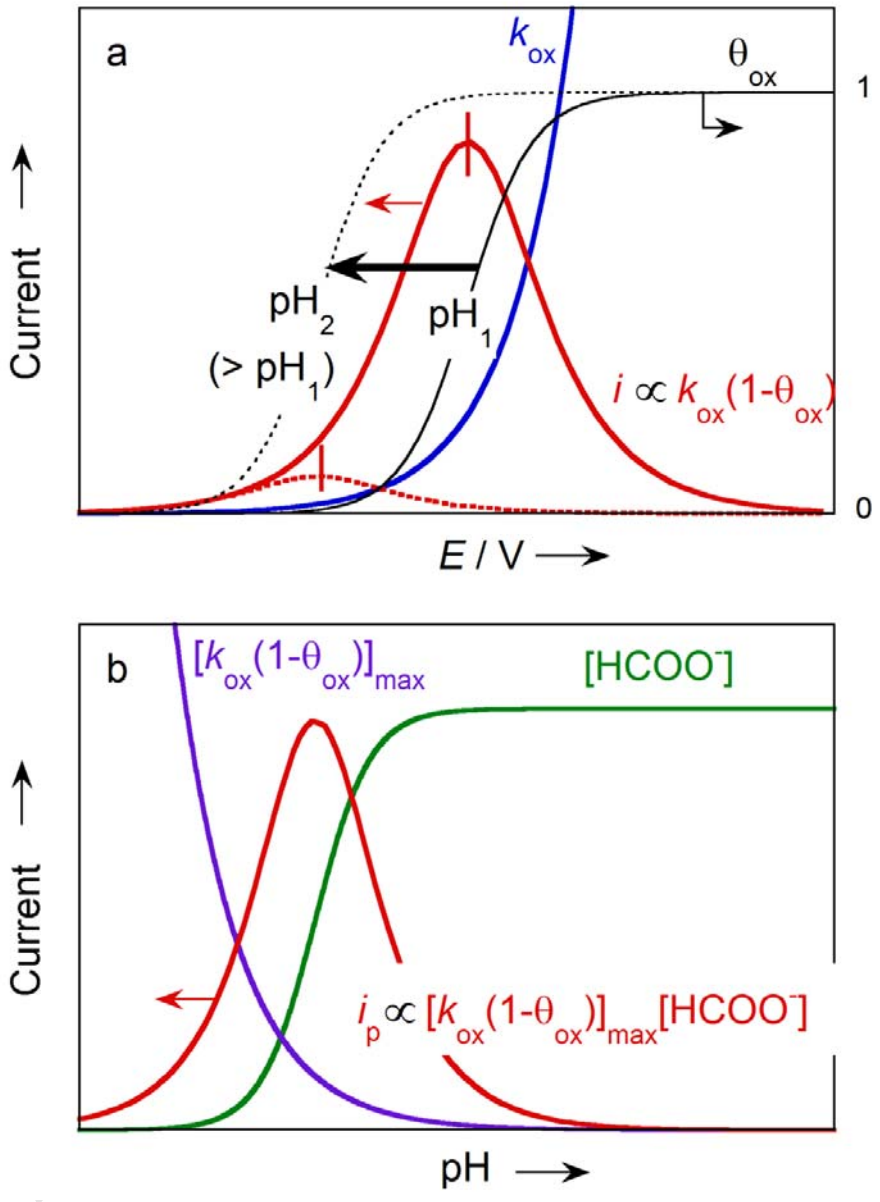

Fig. 6. Schematic explanations (a) for the negative shift and the decrease of the $HCOO^-$ oxidation peak associated with an increase of pH from pH_1 to pH_2, and (b) for the pH dependence of the peak current. k_{ox} is the rate constant and θ_{OX} represents the coverage of Pt oxide or adsorbed OH. See further details in the text.

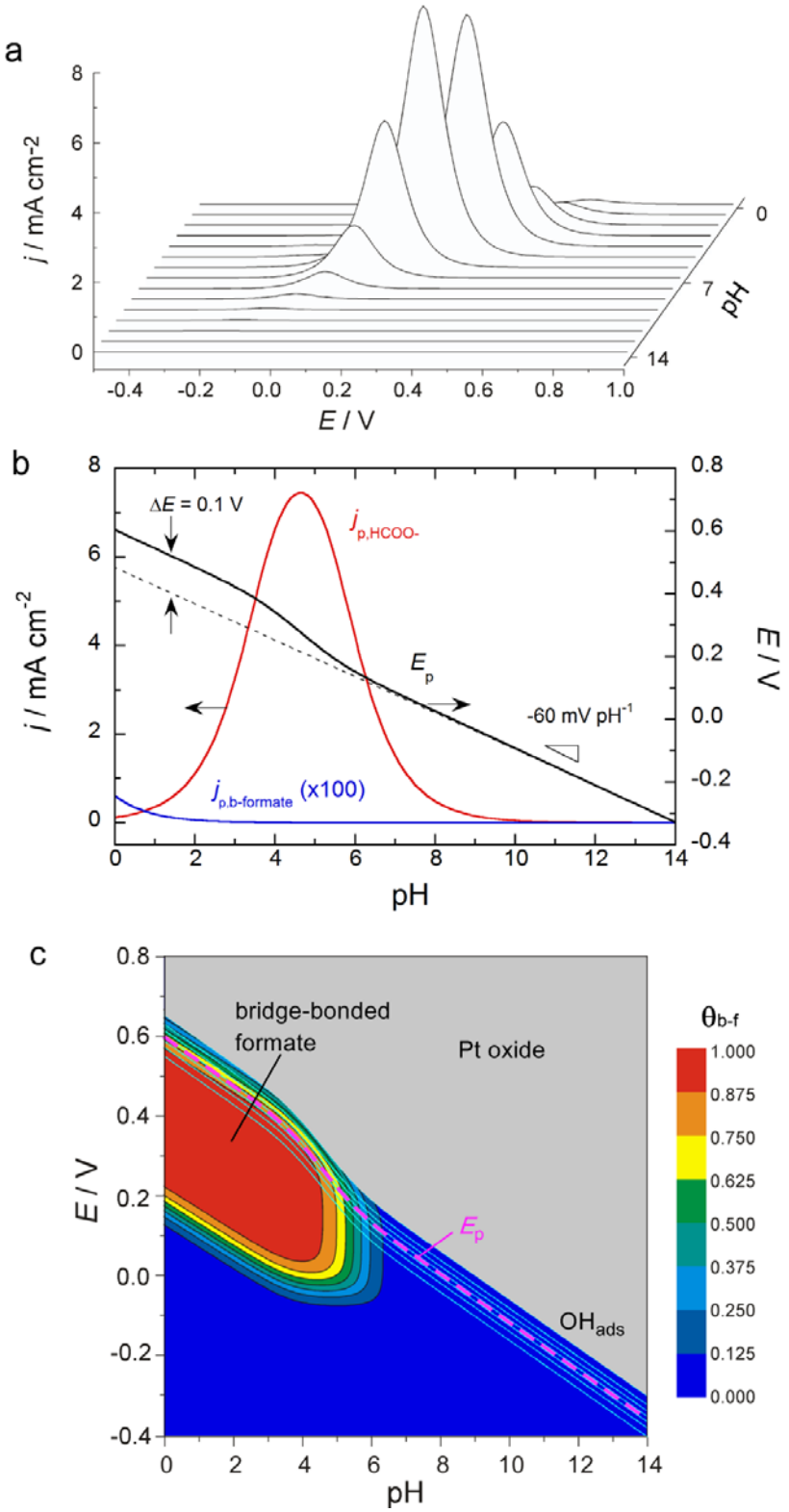

Fig. 7. (a) Simulated pH dependence of the steady-state voltammogram for $HCOOH/HCOO^-$ oxidation. The parameters used were pK_a=3.75, [$HCOOH/HCOO^-$] = 0.1 M, α = 0.5, $k_1^\circ = 8\times10^{-8}$ s^{-1}, $k_3^\circ = 10^{-10}$ mol^{-1} s^{-1}, $k_{-3}^\circ = 10^{-14}$ mol^{-1} s^{-1}, $k_4^\circ = 5\times10^{-16}$ s^{-1}, K_2° = 1 mol^{-1} s^{-1}, E_1° = 0 V, E_2° = 0.5 V, E_3° = 0.3 V, and E_4° = 0 V. (b) Simulated pH dependence of peak currents via the direct $HCOO^-$ pathway ($j_{p,HCOO-}$, red trace) and via the bridge-bonded formate pathway ($j_{p,HCOOH}$, blue trace), and of the peak potential E_p (black solid trace). The dotted straight line is the pH dependence of E_p when bridge-bonded adsorbed formate is absent from the electrode surface. (c) Potential and pH dependece of the coverage of bridge-bonded formate (colored contor plot) and adsorbed OH (light blue contor plot). The dashed pink line is the pH dependece of E_p (same as that in (b)).

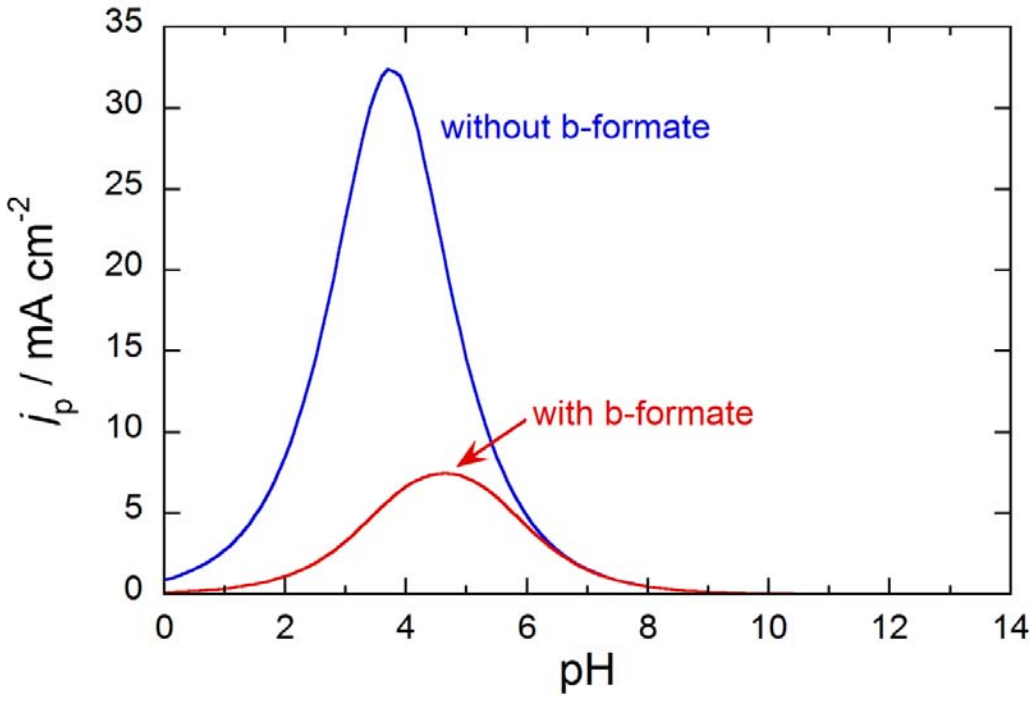

Fig. 8. Simulated pH dependence of peak currents in the presence (red curve) and absence (blue curve) bridge-bonded adsorbed formate. The parameters used were the same as in Fig. 7, but the coverage of bridge-bonded adsorbed formate, $\theta_{b\text{-}f}$, was set zero in the latter.

Graphical abstract